CHAPTER 3

DESCRIPTION OF THE EXPERIMENTAL MODEL

3.1 Introduction

The results of the experimental investigation conducted by Elsaigh (2001) is utilised to appraise the finite element model developed for SFRC ground slabs. The aim of the investigation was to compare the performance of SFRC and plain concrete ground slabs subject to a static load. Only information relevant to SFRC is adapted and presented here, including results obtained from a static test on the SFRC ground slab, plate-bearing test on the support layers (foamed concrete), beam-bending tests, cube tests and cylinder tests. The results for an additional test carried out to establish the compressive stress-strain relationship for the foamed concrete is also presented. It should be noted that experimental results from various other research are utilised but will be presented in following chapters.

3.2 Materials for concrete mixture

SFRC was manufactured by adding 15 kg/m^3 of steel fibres to the concrete mix indicated in Table 3-1. The steel fibres used in this investigation (HD 80 /60 NB) were hook-end wires with an aspect ratio (length/diameter) of 80, length of 60 mm and a tensile strength of 1100 MPa.

Table 3-1: Mix composition for the concrete matrix.

Material	Mass (kg/m^3)
Portland cement	282
Water*	194
Fly ash (unclassified)	78
19 mm stone (granite)	883
13 mm stone (granite)	222
Crusher sand (granite)	662
Filler sand	72

*Water-reducing agents were used

3.3 Slab test setup

A SFRC slab measuring 3000 x 3000 x 125 mm was cast on a foamed concrete slab resting on a deep concrete floor. The dimensions of the SFRC slab and the support layers are shown in Figure 3-1. The foamed concrete was chosen as a support material because it can readily be moulded and kept bound until the end of the experiment. This was not possible with soil as confining boundaries are necessary to contain earth layers. The foamed concrete and SFRC slabs were cast in a shaded area and were covered by plastic sheets for 28 days before the tests were conducted. Testing was conducted using a closed-loop testing system applying displacement at a rate of 1.5 mm/min. The load was applied using a hydraulic twin jack pressing on a stiffened loading plate (100 x 100 mm). The vertical displacements were measured by using Linear Variable Displacement Transducers (LVDT). The LVDTs were mounted on a steel beam spanning over the tested slabs.

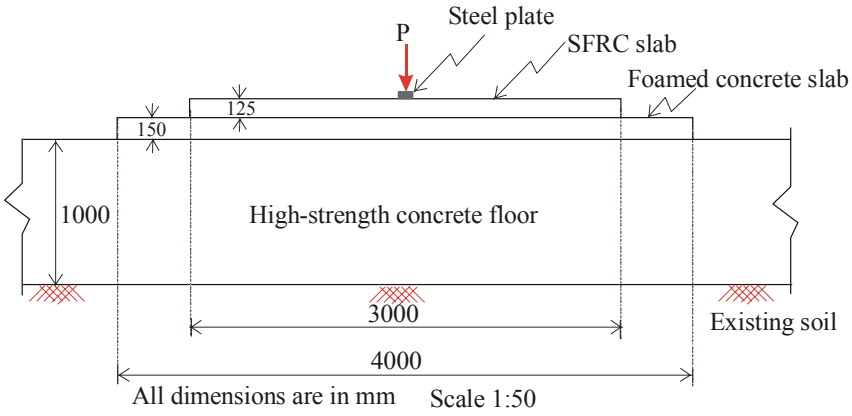

Figure 3-1: Layout of the slab test.

3.3.1 Plate-bearing test

A foamed concrete slab with casting density of 780 kg/m^3 and measuring 8000 x 4000 x 150 mm was cast on a concrete floor surface. The length of the slab was 8000 mm because the foamed concrete slab was also used to support a plain concrete slab constructed adjacent to the SFRC slab. The plate test was performed at the centre of the foamed concrete slab (between the concrete slabs) thus preventing the densification of the support below both the SFRC and plain concrete slabs, which would have influenced the results of the slab test. A plate-bearing test was conducted to establish the load-displacement response (P-Δ) of the supporting material. A circular steel plate with a diameter of 250 mm and a thickness of 40 mm was used.

Figure 3-2 shows the resulting P-Δ response from the plate-bearing test. It should be noted that this response represents the behaviour of all the support layers together, including the interaction

between these layers, and not only the foamed concrete slab. The value of the modulus of the subgrade reaction is determined as 0.25 MPa/mm. This is a relatively high value compared to the values used for support layers made from soil materials often used for road pavements. The range of values used for cement-stabilised soils is between 0.02 and 0.245 MPa/mm (Marais and Perrie, 2000). Both the stiffness of the foamed concrete and the rigid deep floor below the foamed concrete played a role resulting in this high value for the modulus of the subgrade reaction.

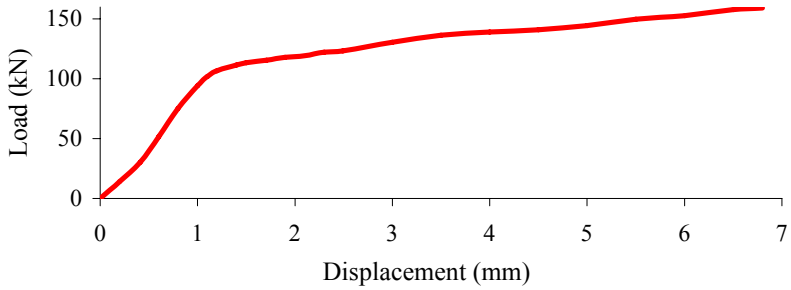

Figure 3-2: Load-displacement response from the plate-bearing test.

3.3.2 SFRC slab test

Figure 3-3 shows the setup for the slab test. The load was applied on a stiffened loading plate, measuring 100 x 100 mm, placed in the centre of the slab.

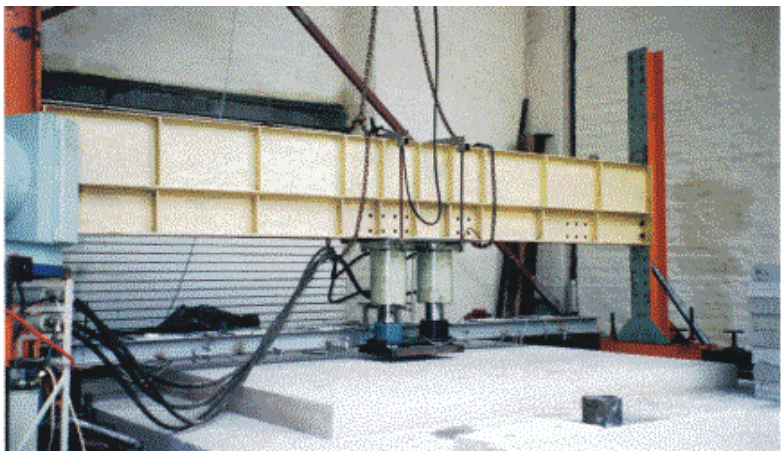

Figure 3-3: Photo shows the set up for slab test.

The resulting *P-Δ* response is indicated in Figure 3-4. The SFRC slab sustained a maximum load at a displacement of approximately 5 mm. Thereafter the load starts to decline. The maximum load maintained in the test is approximately 655 kN.

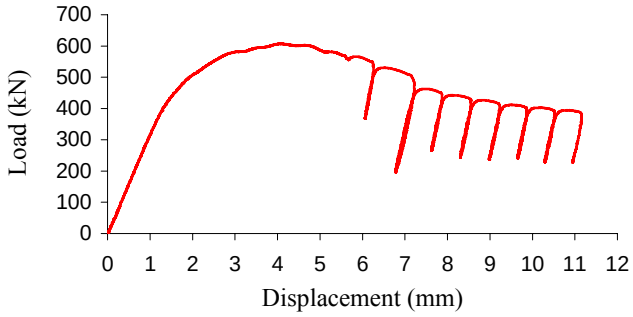

Figure 3-4: The measured load-displacement response of the SFRC slab tested by Elsaigh (2001).

3.4 The beam test

Three beam specimens measuring 750 x 150 x 150 mm were cast using the same SFRC used for the SFRC slab. The specimens were water cured for 28 days before testing. The beam tests were conducted using a closed-loop Material Testing System (MTS) applying displacement at a rate of 0.02 mm/ second. The test set-up is shown in Figure 3-5. Mid-span deflections were measured by using two LVDTs. The readings were taken at 100 Hz. The load was applied by using two bearing rollers (one of them is a swivelling roller) 150 mm apart with their centre line coinciding with the centre of the beam. The beam supports were 450 mm apart and bolted to the MTS testing bed. The beams were cast and tested in accordance to the procedure prescribed by the Japanese Concrete Institute (1983).

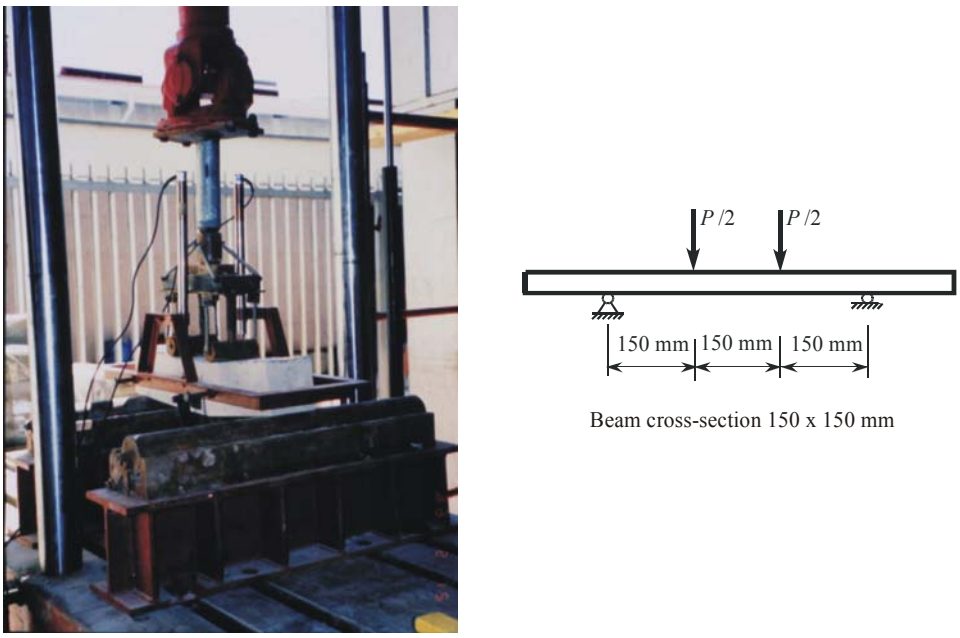

Figure 3-5: Test setup for the beam-bending test.

Figure 3-6 shows the resulting P-δ response for the SFRC beams. Three behavioural stages can be identified. In the second stage no data points were recorded (refer to the dotted line). This is because the sequence of testing at this stage during the loading of the beam is faster than the recording capability of the testing machine.

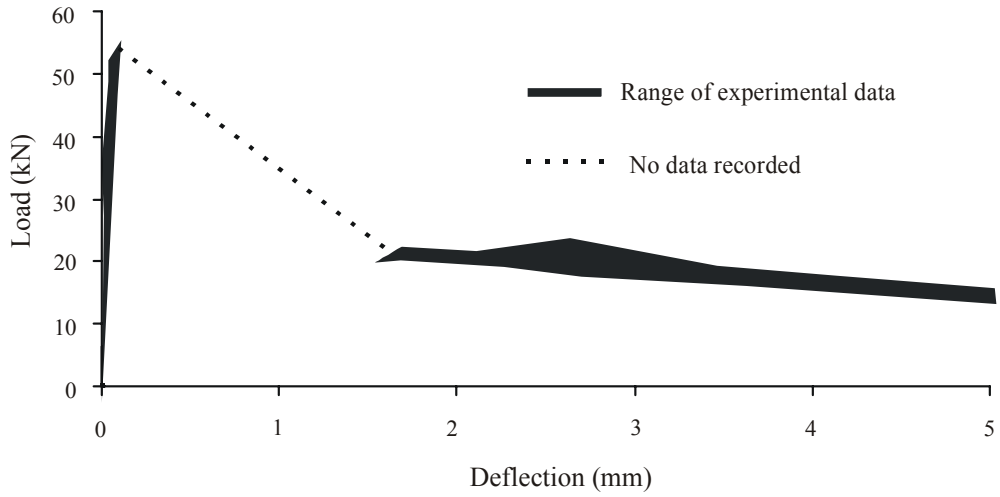

Figure 3-6: The load-deflection responses for the SFRC beams (Elsaigh, 2001).

Figure 3-7 shows the failure mode for the tested SFRC beams. The final failure is dominated by a single major crack occurring at a plane close to the plane of symmetry. Although the beams have cracked, they still did not disintegrate into two parts. This is due the bridging effect provided by the steel fibres across the crack.

Figure 3-7: photo shows the failure mode for the tested beams.

3.5 Cube and cylinder tests

Three cubes (150 x 150 x 150 mm) and two cylinders (150 diameter and 300 mm length) were manufactured from the same material used in the SFRC slab and beams. They were water cured for 28 days before testing. The cubes were tested according to the procedure prescribed by Standard Method: SABS Method 863:1994(1994) while the cylinders were tested according to the procedure prescribed by the ASTM C 469-94a (1992). Six cores, with a 100 mm diameter, were taken from different positions after the testing the SFRC slab. The cores were drilled, prepared and tested according to SABS Method 865 (1982). The core strengths were converted to actual standard cube strength using the conversion formula given in the British Concrete Society Technical Report No. 11 (Neville and Brooks, 1998). Apart from the cylinder test, the Young's modulus is also estimated using the results of the beam-bending test. The formula derived by Alexander (1982) is utilised as indicated in Equation 3-1. The average results are summarised in Table 3-2.

Table 3-2: Compressive strength and Young's modulus.

Cube strength (MPa)	47
Core strength (MPa)	52
Young's modulus (GPa) (Cylinder tests)	27
Young's modulus (GPa) (Beam-bending tests)	28

$$\mathrm{E\,(MPa)} = \frac{23}{1296}.\frac{P}{\delta}.\frac{L^3}{I}\left[1+\frac{216}{115}.\left(\frac{\mathrm{d}}{L}\right)^2.(1+\mu)\right].10^3 \qquad (3\text{-}1)$$

$\frac{P}{\delta}$ = The slop of the linear elastic part on the load-deflection response (N/mm^2).

L = The supported span of the beam (mm).

I = The second moment of area of the beam cross-section ($\frac{\mathrm{bh}^3}{12}$) (mm^4).

b, h = The width and depth of the beam respectively (mm).

μ = Poisson's ratio.

CHAPTER 4

MODELLING NON-LINEAR BEHAVIOUR OF STEEL FIBRE REINFORCED CONCRETE

4.1 Introduction

The availability of steel fibres with a variety of physical and mechanical properties, as well as the use of various fibre contents, tend to complicate prediction of the tensile stress-strain (σ-ε) response of SFRC. The further complexities of testing concrete in direct tension and measuring stresses and strains may be the reasons for the many proposed material models for SFRC. However, the current international drive for establishing tensile σ-ε relationship for SFRC has shifted towards inverse analysis (back-calculation) techniques. In these techniques flexural response obtained from beam-bending test is used to back-calculate tensile σ-ε relationship. Elsaigh et al. (2004) proposed a method to determine the tensile σ-ε relationship for SFRC utilising experimental results obtained from beam third-point tests. Alena et al. (2004) have concurrently proposed a similar method. Østergaard and Olesen (2005) and Østergaard et al. (2005) have recently proposed an inverse analysis method that is based on the non-linear hinge concept described by Olesen (2001). This method does however fall beyond the scope of this study.

In this chapter a generalised analytical method is proposed to determine the tensile σ-ε response for SFRC. In this method the σ-ε relationship is determined from either the experimental moment-curvature (M-ϕ) or load-deflection (P-δ) responses. A parameter study is conducted to not only investigate the influence of each of the tensile σ-ε curve parameter on the M-ϕ and the P-δ responses but also to serve as an aid to the user in adjusting the tensile σ-ε parameters.

4.2 Analysis method

In the analysis the M-ϕ and the P-δ responses are derived by assuming a σ-ε response. A trial and error technique is followed, by adjusting the σ-ε relationship until the analytical results fit the experimental results for either M-ϕ or P-δ. In the analysis, the following three-step procedure is used to calculate the P-δ response of SFRC beams:

(1) Assume a σ-ε relationship for the SFRC.

(2) Calculate the M-ϕ response for a section; and

(3) Calculate the P-δ response for an element.

At the end of either steps (2) or (3) the results from the analysis are compared to experimental results and adjustments are made to the σ-ε response until the analytical and experimental results agree within acceptable limits.

4.2.1 Proposed stress-strain relationship

The shape of the proposed σ-ε relationship used in this analysis is shown in Figure 4-1. The tensile response is similar to that proposed by RILEM TC 162-TDF (2002) while the compression response is assumed linear elastic up to a limiting strain ε_{c0}.

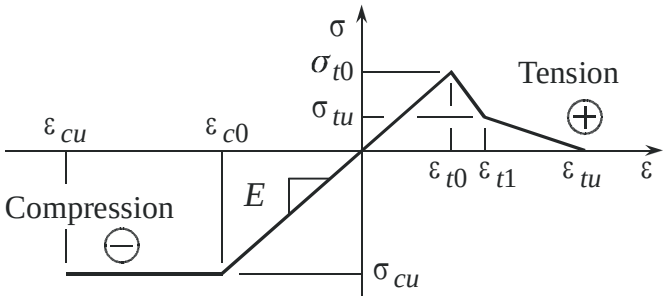

Figure 4-1: Proposed stress-strain relationship.

In Figure 4-1, σ_{t0} and ε_{t0} represents the cracking strength and the corresponding elastic strain. σ_{tu} and ε_{t1} represents the residual stress and the residual strain at a point where the slope of softening tensile curve changes. ε_{tu} is the ultimate tensile strain. E is Young's modulus for the SFRC. σ_{cu} and ε_{co} are the compressive strength and the corresponding elastic strain. ε_{cu} is the ultimate compressive strain.

The σ-ε relationship is expressed as follows:

$$\sigma(\varepsilon) = \begin{cases} \sigma_{cu} & \text{for } (\varepsilon_{cu} \le \varepsilon < \varepsilon_{c0}) \\ E\varepsilon & \text{for } (\varepsilon_{c0} \le \varepsilon < \varepsilon_{t0}) \\ \sigma_{t0} + \psi(\varepsilon - \varepsilon_{t0}) & \text{for } (\varepsilon_{t0} \le \varepsilon < \varepsilon_{t1}) \\ \sigma_{tu} + \lambda(\varepsilon - \varepsilon_{t1}) & \text{for } (\varepsilon_{t1} \le \varepsilon < \varepsilon_{tu}) \end{cases} \qquad (4\text{-}1)$$

Where: $E = \dfrac{\sigma_{cu}}{\varepsilon_{c0}}$

$$\psi = \frac{\sigma_{tu} - \sigma_{t0}}{\varepsilon_{t1} - \varepsilon_{t0}}$$

$$\lambda = \frac{-\sigma_{tu}}{\varepsilon_{tu} - \varepsilon_{t1}}$$

4.2.2 Moment-curvature response

The M-ϕ relationship at a section is calculated by making use of the following assumptions:

- The σ-ε relationship of the material is known.
- Plane sections perpendicular to the centre plane in the reference state remain plane during bending.
- Internal stress resultants are in equilibrium with the externally applied loads.

As part of the first assumption, the σ-ε relationship proposed in equations (4-1) is used and initial values are assumed for the parameters. The second assumption applies to slender beams and implies a linear distribution of strain so that the following relationships exists at a section (see Figure 4-2b):

$$\varepsilon(y) = \frac{y}{a}\varepsilon_{top} = \left(\frac{y}{h-a}\right)\varepsilon_{bot} \tag{4-2}$$

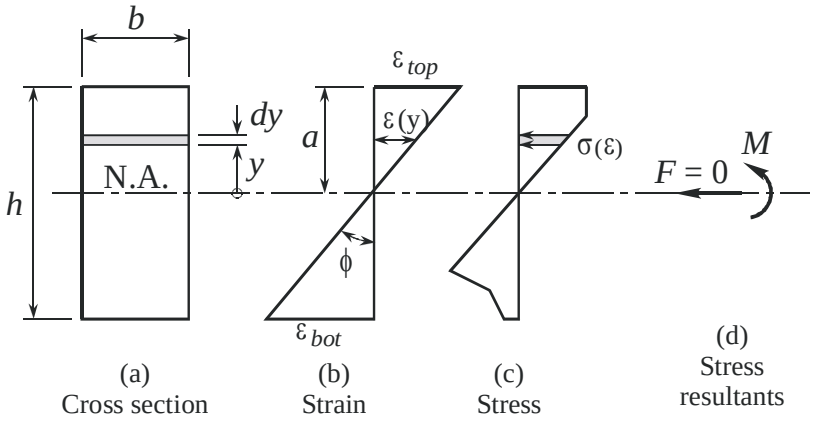

Figure 4-2: Stress and strain distributions at a section.

The final assumption is used to find the axial force F (which is equal to zero) and moment M (which is equal to the applied moment):

$$F = \int_{-(h-a)}^{a} \sigma(\varepsilon)\, b\, dy = \frac{a\,b}{\varepsilon_{top}} \int_{\varepsilon_{bot}}^{\varepsilon_{top}} \sigma(\varepsilon)\, d\varepsilon = 0 \tag{4-3}$$

$$M = \int_{-(h-a)}^{a} \sigma(\varepsilon)\, y\, b\, dy = -\frac{a^2\, b}{\varepsilon_{top}^2} \int_{\varepsilon_{bot}}^{\varepsilon_{top}} \sigma(\varepsilon)\, \varepsilon\, d\varepsilon \tag{4-4}$$

At a typical section there are two unknowns necessary to describe the strain distribution. For a given strain distribution the stresses at a section (see Figure 4-2c) can be calculated using the σ-ε relationship and equations (4-3) and (4-4) can be used to solve the two unknowns. The curvature at a section is given by:

$$\phi = \frac{\varepsilon_{top}}{a} = \frac{\varepsilon_{bot}}{(h-a)} \qquad (4\text{-}5)$$

The following procedure is followed to obtain the M-ϕ relationship:

(1) A value is selected for the bottom strain ε_{bot}.

(2) The top strain ε_{top} is solved from equation (4-3) by following an iterative procedure in which ε_{top} is changed until $F = 0$.

(3) M and ϕ is calculated from equations (4-4) and (4-5) respectively. This produces one point on the M-ϕ diagram.

(4) A new ε_{bot} is selected and steps (1) to (3) are repeated to until sufficient points have been generated to describe the complete M-ϕ relationship.

4.2.3 Load-deflection response

The total deformation of a beam consists of two components: that is extension caused by the moments (ε.dx) and shear distortion (γ.dx) caused by the shear force (Refer to Figure 4-3).

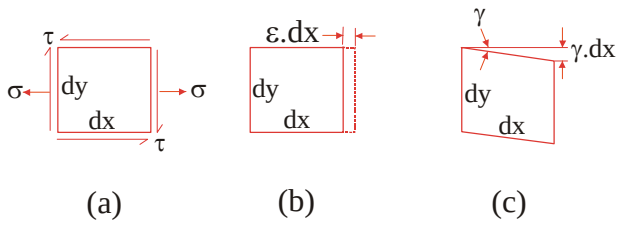

Figure 4-3: Differential element from the beam.

Because the effects of shear deformations on deflection of beams are usually relatively small compared to the effects of flexural deformations, it is common practice to disregard them. However for short beam specimens of the type normally specified for laboratory testing, the span-depth ratio lies in the range of 3 to 4 and therefore shear stresses will contribute significantly to the total deflections of the beam. At any loading point during the loading process, the total deflection of a beam (δ) is estimated as the sum of the deflection due to moments (δ_m) and the deflection due to shear forces (δ_V). The unit-load method is used to obtain the total deflection by integrating curvature ($\phi = M/EI$) and shear strain ($\gamma = V.f_{sh}/GA$) along the beam (Refer to Equation 4-6).

$$\delta = \delta_m + \delta_V = \int_0^L \frac{M_u M_L .dx}{EI} + \int_0^L \frac{V_u V_L .dx}{GA/f_{sh}} \qquad (4\text{-}6)$$

Where: M_u and M_L are the moments due to a unit load and actual load respectively, EI is the flexural rigidity, V_u and V_L are shear forces due to unit load and actual load respectively, GA/f_{sh} is the shearing rigidity of the beam (Gere and Timoshenko, 1991), f_{sh} is the factor for shear (equals 6/5 for rectangular section).

The deflections due to moments (δ_m) are calculated from the distribution of the curvature due to moment (ϕ) along the beam where ϕ replaces $\frac{M_u}{EI}$ in Equation (4-6). Consider the beam in Figure 4-4(b) subjected to a variable load *P*. For moments up to the maximum moment M_m the curvature is obtained from the *M*-ϕ relationship in Figure 4-4(a) yielding the dashed line in Figure 4-4(b). Beyond this point the analysis effectively switches to displacement control. It is assumed that material having reached M_m (part BC of the beam) will follow the softening portion of the *M*-ϕ relationship. For example; if the curvature in BC increases to ϕ_c, the moment will reduce to M_c. Equilibrium requires the moments in parts AB and CD of the beam to reduce and the material here is assumed to unload elastically, producing smaller curvatures for these parts. This is because tensile stresses on the end thirds of the beam decrease as the crack width in the middle third increases.

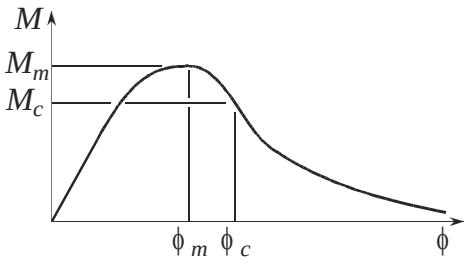

(a) Moment-curvature relationship

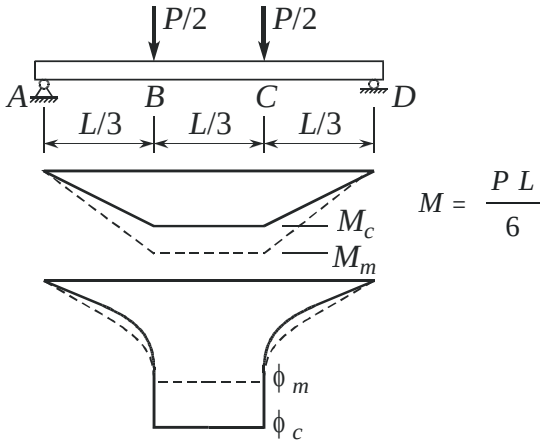

(b) Moment and curvatures distributions for an applied load *P*

Figure 4-4: Finding the moment-curvature distribution along the beam.

The deflections due to shear forces (δ_V) are calculated from the distribution of the shear strain (γ) along the beam. Referring to the load configurations shown in Figure 4-5(b), the shear deflection in the beam is due to the shear forces in part AB and CD. The fact that these two parts unload elastically at the onset of the flexural cracks in part BC has resulted in less complexities compared to that followed for the M-ϕ analysis. At any stage throughout the loading process of the beam, shear strains on the $V-\gamma$ response shown in Figure 4-5(a) are calculated using the measured P-δ response by dividing the shear force by the shearing rigidity. This means the effect of shear forces on deflection increases to reach the maximum at the peak load and decreases with increasing displacement beyond this peak load.

The distribution of elastic shear strain (γ) through the depth of beams with un-cracked rectangular sections is parabolic. As a result of shear strains, cross-sections of the beam that were originally plane surfaces become warped. For the beam set up in Figure 4-4(b) and Figure 4-5(b), the shear deformation is zero in the constant moment zone (BC). For this reason, it is justifiable to use the bending formula derived for pure bending. The effects due to shear and moment were calculated separately. The superposition concept was used to calculate the total deflection as the sum of both effects. Therefore, the approach used is deemed to be sufficiently accurate. Care should be taken when using this approach to calculate the P-δ response for beams having different loading configurations.

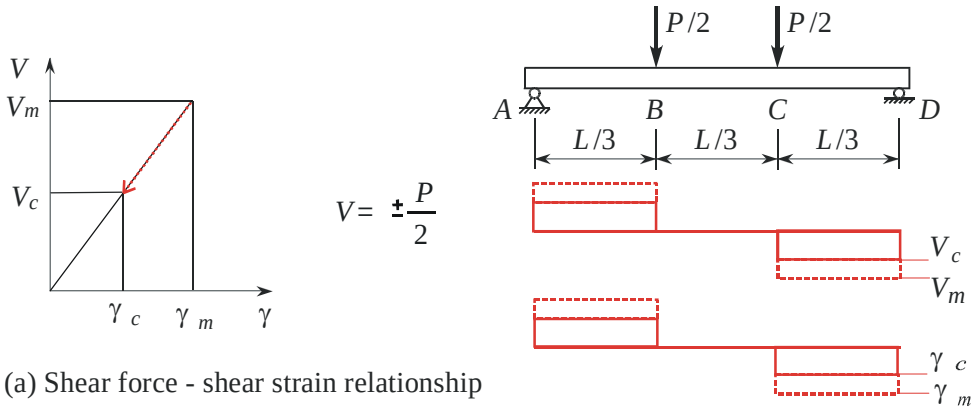

(a) Shear force - shear strain relationship

(b) Shear forces and shear strain distributions for an applied load P

Figure 4-5: Finding the shear-shear strain distribution along the beam.

It is generally accepted that the area under the tensile σ-ε curve represents the fracture energy. The characteristics of the softening part of the tensile σ-ε curve is largely dependent on the size of the

element in which the crack occurs. When calculating the P-δ response using the method presented here, the beam was divided into three elements and the crack was smeared over the constant moment zone (part BC of the beam). It was also assumed that an infinite number of layers (elements) exist through the depth of the beam. Therefore element size should carefully be selected when using the calculated tensile σ-ε curve in finite element analysis.

4.2.4 Implementation of the analysis method

The experimental results obtained by Lim et al. (1987 a and b) are used to implement and test the proposed analysis method by comparing calculated M-ϕ and P-δ responses to the experimental results. In their experimental programme, SFRC specimens were tested in compression, direct tension and flexure. Two series each of four mixes were cast. Only results of specimens containing 0.5 percent by volume (40 kg/m^3) of hooked-end steel fibres, with 0.5 mm diameter and 30 mm length, are discussed here. Figure 4-6 indicates the specimen size and test set up for direct tension and flexural tests. The tensile specimens were tested in direct tension by a pair of grips on a servo-controlled testing machine. The extension rate was set at 0.25 mm / min. The extensions were monitored over a gage length of 200 mm. The flexural beam tests over a simply supported span of 750 mm and loaded at the third-point (refer to Figure 4-6(b)). The P-δ response was established directly from the measurement. The curvature was derived from the strain readings using electrical gages bonded onto the top and bottom faces of the beam. The average compressive strength and Young's modulus for the SFRC were determined as 34 MPa and 25.4 GPa respectively.

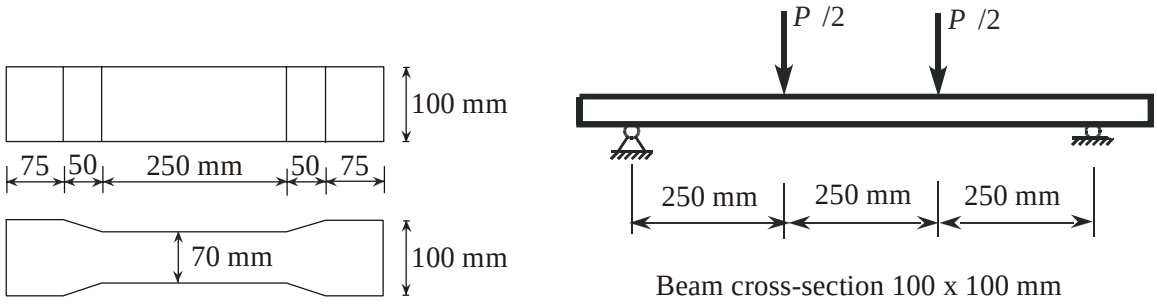

(a) Direct tension specimen

(b) Test set up for flexural test

Figure 4-6: Direct tension and flexural specimens tested by Lim et al. (1987 a and b).

The method proposed here was set up using Mathcad (2001). The shape of the tensile σ-ε relationship is assumed as in Figure 4-1. The first estimation of for σ_{t0}, ε_{t0}, σ_{tu}, ε_{t1}, and ε_{tu} is made based on the results of the direct tension test. A trial-and-error procedure is followed to adjust these parameters until the calculated M-ϕ and P-δ responses match the experimental responses (refer to

Appendix B). Figure 4-7 shows the tensile σ-ε relationships predicted using the analysis method and measured from direct tension test. Note that no experimental data were recorded immediately beyond the maximum tensile stress.

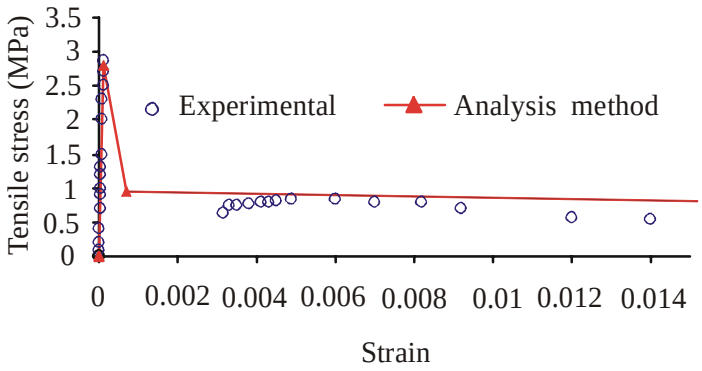

Figure 4-7: Assumed tensile stress-strain relationship for comparison to experimental results of Lim et al. (1987 b).

Figure 4-8 shows the correlations between calculated and experimental M-ϕ and P-δ responses. The analyses show some similarity between the shapes of the σ-ε relationship, the M-ϕ and P-δ responses although they differ in magnitude. The analysis has however shown that the point where the maximum tensile stress (2.8 MPa) in the material is first reached occurs in the pre-peak regions of both the M-ϕ and P-δ responses (see the arrows of Figure 4-8). This means that to utilise the full tensile capacity of the material, the analysis should incorporate the non-linear material properties.

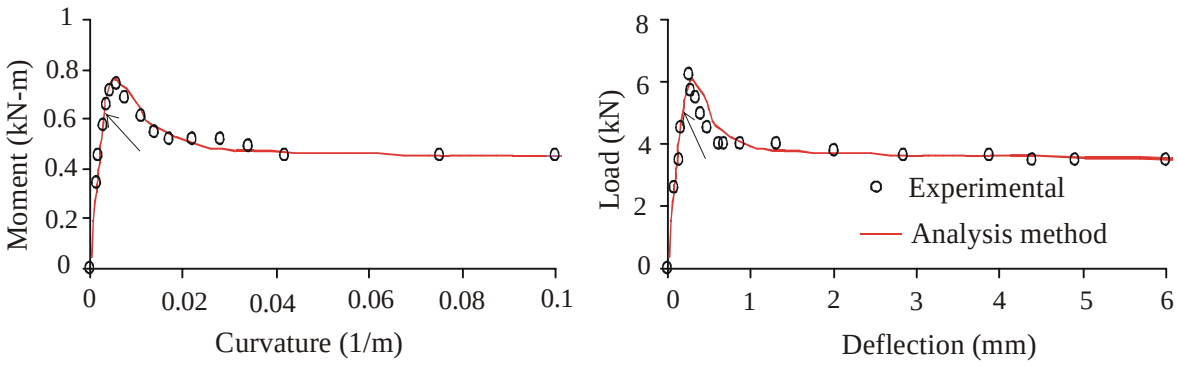

Figure 4-8: Experimental (Lim et al., 1987 a) and calculated M-ϕ and P-δ responses.

Figure 4-9 shows the comparison between tensile σ-ε relationships, developed using the various models, and the resulting M-ϕ responses. The models proposed by Lim et al. (1987 a), Nemegeer

(1996) and Lok and Xiao (1998) were used to determine the tensile σ-ε relationship for the SFRC tested by Lim et al. (1987a). The comparison excluded the models developed by Vandewalle (2003) and Dupont and Vandewalle (2003), as they require results from notched beam test.

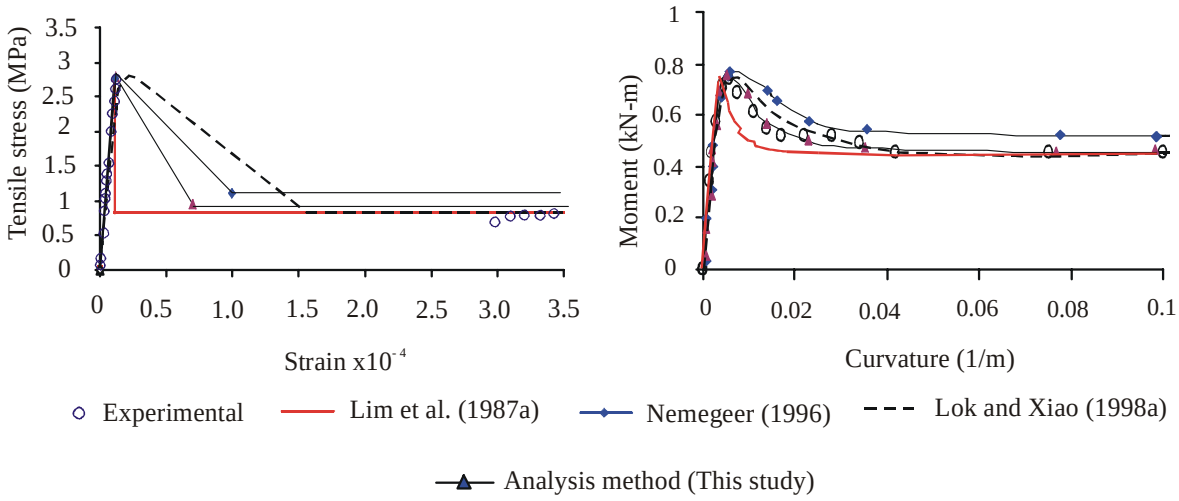

Figure 4-9: Correlation between tensile stress-strain responses determined using various models.

The main difference between these four models is the value of the residual strain (ε_{t1}), The assumption made in the model of Lim et al. (1987 a) where ε_{t1} is equal to the cracking strain (ε_{t0}) resulted in a larger divergence between the experimental and calculated M-ϕ response in the region immediately beyond the maximum moment. The higher value for σ_{tu} determined using the model of Nemegeer (1996) resulted in an increased moment for the last part of the M-ϕ response.

Figure 4-10 shows the contribution of deflections due to shear as percentage of the total deflection. The percentage of shear deflections up to the cracking point (ε_{t0}) is constant at approximately 4 percent. The contribution of shear deflection varies significantly beyond the cracking point of the beam and it decreases to approximately 0.2 percent at the point of residual strain (ε_{t1}).

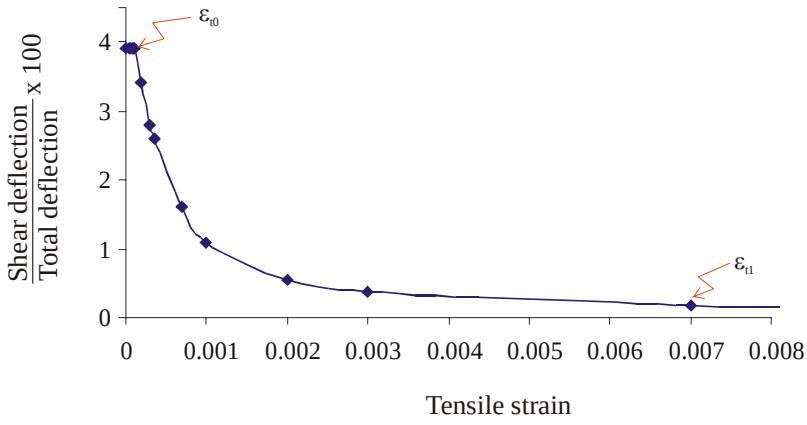

Figure 4-10: Contribution of shear deflection to the total deflection of the beam.

For the beam with the dimensions and setup shown in Figure 4-6 (b), the contribution of shear to the total deformation of the beam is negligible. This is not surprising as the span-depth ratio for this beam is 7.5, which is sufficiently large to alleviate the effect of shear stresses on the mid-span deflection. However, for deeper beam specimens the effect of shear deflection will be more pronounced. For example, a beam measuring 150 x150 x 750 mm loaded at its third points and supported over a span of 450 mm will result in a maximum shear deflection approximately 18 percent of the total shear refer to Appendix C). Thus shear deformation can be crucial with respect to the tensile σ-ε relationship as the former is back calculated by fitting measured and calculated P-δ responses.

The merit of the analysis procedure presented here is that it uses measured M-ϕ or P-δ responses obtainable with minimal testing complexities compared to procedures requiring results from direct tensile tests. In addition, the method utilises a macro approach as the influence of the steel fibre parameters and the concrete matrix are reflected in the measured M-ϕ or P-δ responses. This is seen as an advantage compared to procedures utilising a micro approach in which the fibre properties, the concrete matrix properties and the fibre-matrix interaction have to be known.

4.3 Parameter study

The parameter study is conducted by changing parameters on the tensile σ-ε curve and then calculating M-ϕ and P-δ responses using the analytical method described in section 4.2. The parameters that define the tensile σ-ε of the SFRC (see Figure 4-1) are:

- Cracking strength σ_{t0} and corresponding cracking strain ε_{t0},
- Residual stress σ_{tu} and corresponding strain ε_{t1}, and
- Ultimate strain ε_{tu}.

In the analysis, only one parameter will be changed at a time while keeping all the other parameters fixed. The main objective of the parameter study is to investigate the influence of the σ-ε parameters on M-ϕ and P-δ responses. Subsequently, a systematic approach can be followed leading to a faster arrival at the material σ-ε response. A secondary objective is to give an insight into the behaviour of SFRC.

Hypothetical beams assumed for the parameter study have a section size of 150 x 150 mm and a supported span of 450 mm. A Mathcad (2001) work sheet is set up and prepared to carry out the calculations. Fifteen analyses were conducted (see Appendix B for sample of calculations).

4.3.1 Effect of changing cracking strength or corresponding strain

Figure 4-11(a) shows three σ-ε curves where only the tensile and compressive strengths are changed, while in Figure 4-11(b) only the cracking strains are changed. These parameters are studied together since changes to them also influence Young's modulus. Three values for Young's modulus commonly encountered are investigated viz. 15, 25 and 35 GPa. When changing the cracking strengths, the corresponding compressive strengths are assumed to be ten times the magnitude of the cracking strengths while a reasonable fixed value is assumed when changing the cracking strains.

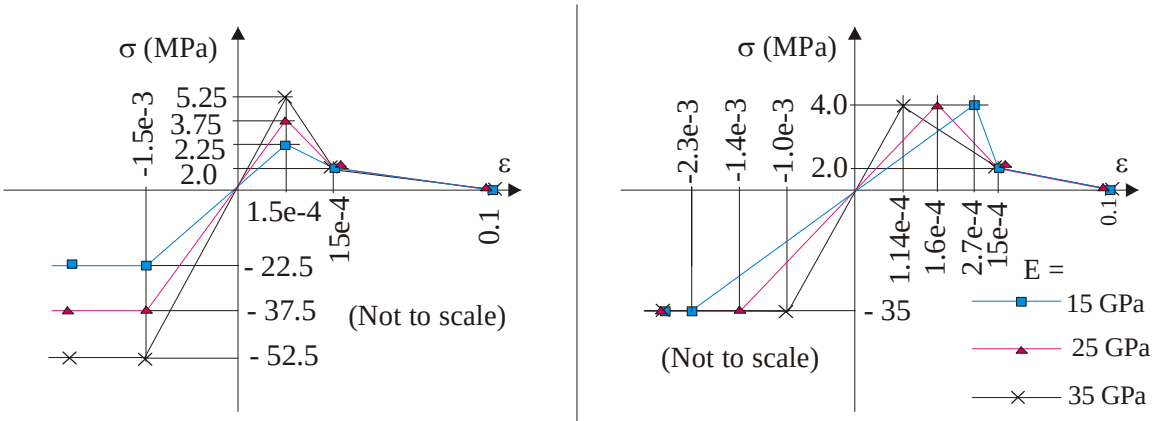

(a) Changing strength (b) Changing elastic strain

Figure 4-11: Stress-strain curves - changing cracking strength and corresponding strain.

The approximation with respect to the ratio between compressive and cracking strength (equals 10) is justified by experimental results reported in other research. For example, Kupfer et al. (1969) reported that the ratio of uniaxial cracking strength to compressive strength of concrete amounts to 0.11, 0.09, and 0.08 for concrete with compressive strength of 19, 31.5 and 59 MPa respectively (refer to Figure 2-12 in section 2.3.5.4). The effect of steel fibres on these ratios is expected to be insignificant. This is because the addition of steel fibre to concrete results in a marginal increase in compressive strength (Burgess, 1992, Elsaigh, 2001) while the steel fibres are only active in tension after the initiation of a crack in SFRC resulting in a negligible, or no increase in cracking strength. The approximations made herein are thus considered reasonable for the types of normal strength concrete often used in pavement applications.

It is worth noting that the relations between tensile and compressive strength, as well as Young's modulus can be significantly different to the approximations considered here, or specifically

engineered to be different, for some other cement-based composites, which is beyond the scope of this research.

Figure 4-12 shows that an increase in tensile and compressive strength (and increase in Young's modulus), results in an increase in the magnitude of peak moment and peak load on the M-ϕ and P-δ curves respectively. For example, increasing the cracking strength by 40 percent (from 3.75 to 5.25 MPa) leads to an increase on the peak load of approximately 36 percent. The pre-peak slope of the curves as well as the slope immediately beyond the peak moment and the peak load become steeper with increased strength. Although the M-ϕ and P-δ curves are curtailed to show only the segments most affected by changing tensile stress, the complete responses indicate that the values of moment and load reduce to zero when the tensile stress on the σ-ε curves reduces to zero.

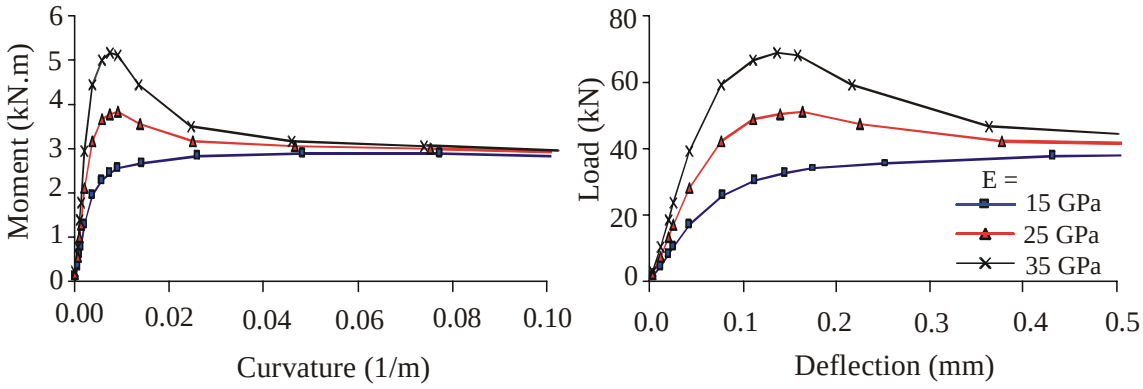

Figure 4-12: Effect of changing strength on M-ϕ and P-δ responses.

Referring to Figure 4-13, an increase in cracking strain (which decreases Young's modulus) results in a decrease in the magnitudes of peak moment and peak load, while also increasing the curvature and deflection corresponding to these peak values. For example, increasing the cracking strain by 69 percent (from 1.6 x10^{-4} to 2.7 x10^{-4}) leads to an increase on the peak load of approximately 1.9 percent. Therefore, the change in the value of cracking strain is considered to result in a negligible change in the values of peak moment and peak load. This also correlates well with the findings presented in Figure 4-9. The slope of the first part of the curves as well as the slope immediately beyond the peak moment and peak load decreases as Young's modulus decreases. The M-ϕ and P-δ curves are curtailed to show only the segments most affected by changing elastic strain (refer to the discussion on Figure 4-12).

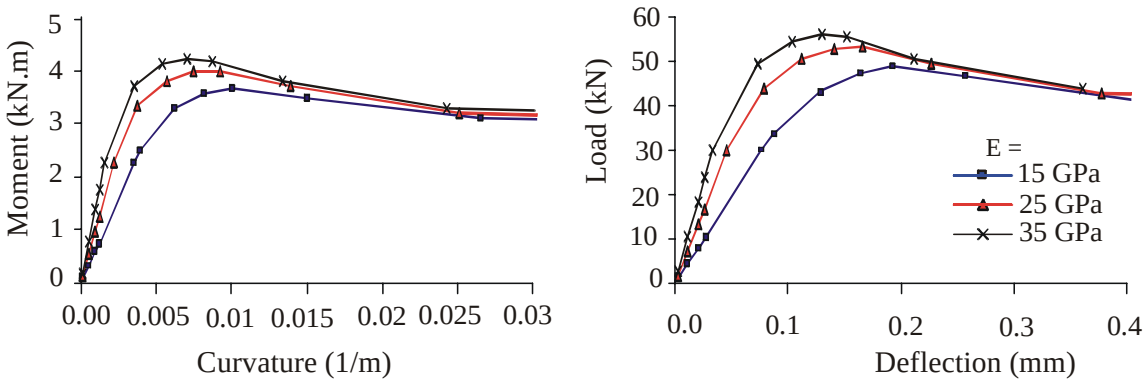

Figure 4-13: Effect of changing elastic strain on M-ϕ and P-δ responses.

4.3.2 Effect of changing residual stress or corresponding strain

Changing the residual stress or the residual strain influences the slope of both curves beyond the cracking strength of the σ-ε curve. On this part of the curve, the steel fibre parameters and content play a major role in the composite tensile behaviour. As indicated in Figure 4-14(a) and Figure 4-14(b), two sets of analyses are performed. In the first set the magnitude of residual stress is changed while in the second set the magnitude of residual strain is changed. A constant compressive strength value, equal to ten times the cracking strength, is assumed in these two sets of analysis.

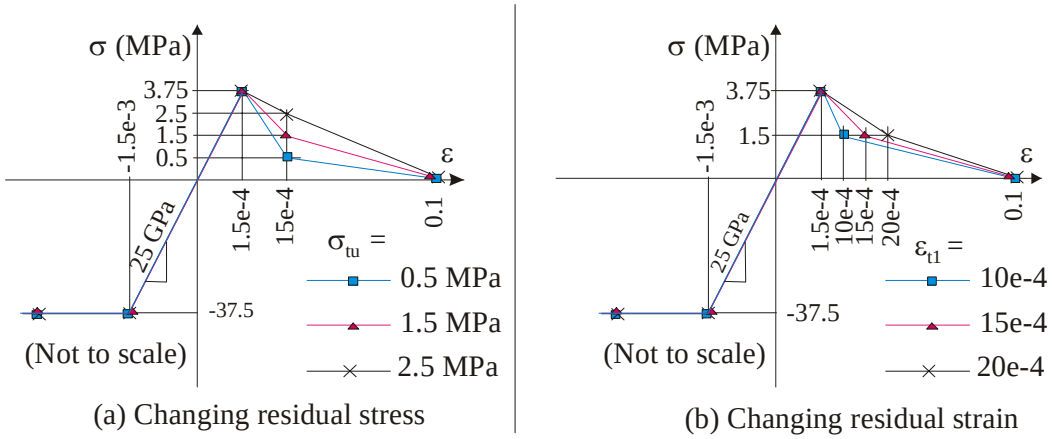

(a) Changing residual stress (b) Changing residual strain

Figure 4-14: Stress-strain curves for SFRC - changing residual stress or residual strain.

Figure 4-15 indicates that increasing the residual tensile stress shifts up the last part of the M-ϕ and P-δ responses while increasing the peak moment and the peak load. The increase in the elevation of the last part is significant while the increase in peak moment and load is little. For example, increasing the residual stress by 67 percent (from 1.5 to 2.5 MPa) increases the elevation of the last

part of the M-ϕ and P-δ responses an increases the peak load by approximately 67 percent and 4 percent respectively. It also flattens the part of the curve immediately beyond the peak moment and the peak load. The M-ϕ and P-δ curves are again curtailed to only show the segments most affected by changes in residual stress (refer to the discussion on Figure 4-12).

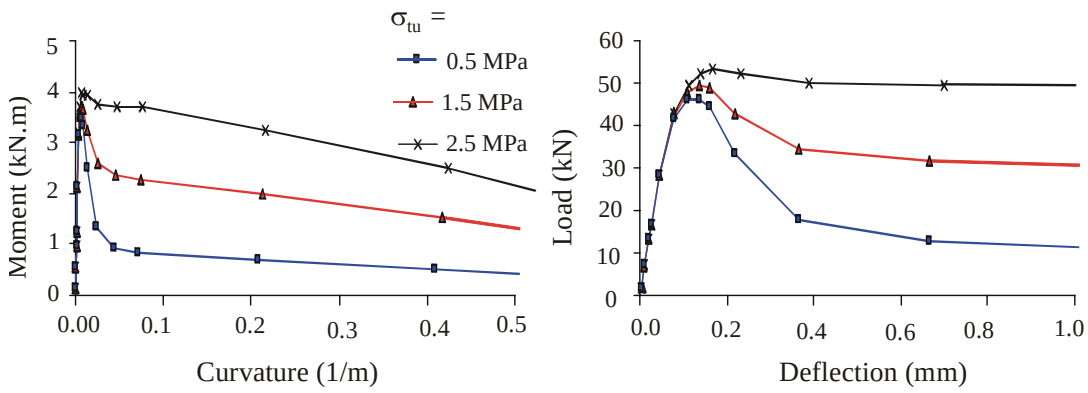

Figure 4-15: Effect of changing residual stress on M-ϕ and P-δ responses.

Figure 4-16 shows that increasing the residual strain increases the peak moment and the peak load as well as the corresponding curvature and deflection. For example, increasing the residual strain by 33 percent (from $15\text{x}10^{-4}$ to $20\text{x}10^{-4}$) leads to an increase in the peak load of approximately 2 percent. In the process of determining the σ-ε relationship, the residual strain can be used to make small corrections to the peak moment, peak load and the corresponding curvature and deflection. The M-ϕ and P-δ curves are one more curtailed to show only the segments most affected by changes in residual strain (refer to the discussion on Figure 4-12).

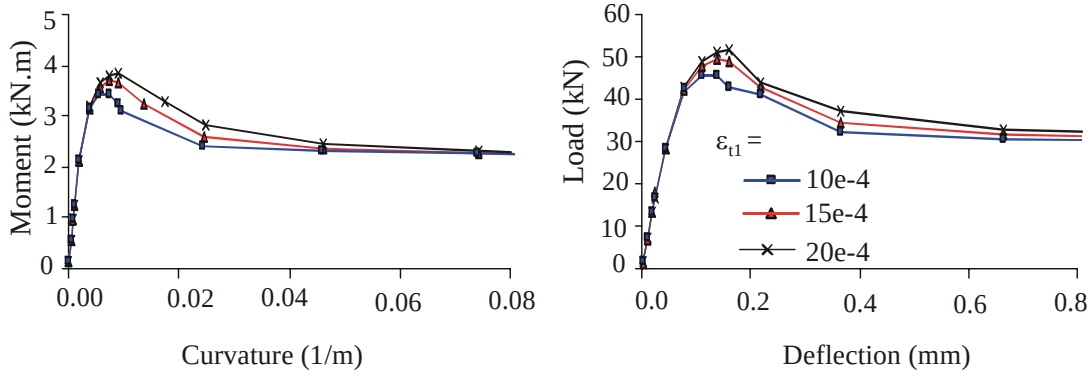

Figure 4-16: Effect of changing residual strain on M-ϕ and P-δ responses.

4.3.3 Effect of changing ultimate strain

Changing the magnitude of the ultimate strain does not influence any other parameter on the σ-ε curve. Figure 4-17 shows three σ-ε relationships for which the ultimate strain is changed while all other parameters are kept constant. A constant compressive strength value equal to ten times the cracking strength is assumed in these two sets of analysis.

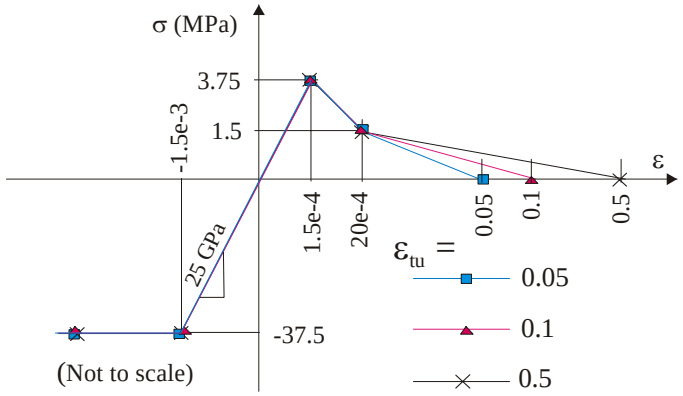

Figure 4-17: Stress-strain curves for SFRC- changing ultimate strain.

Figure 4-18 shows that the magnitude of the ultimate strain only influences the slope of the last part of the M-ϕ and P-δ curves and ε_{tu} can therefore be used to adjust this part of the curve.

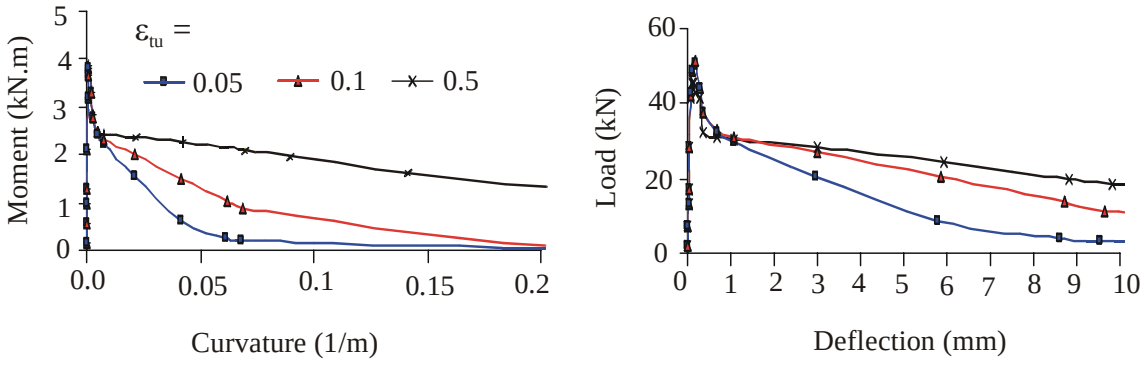

Figure 4-18: Effect of changing ultimate strain on M-ϕ and P-δ responses.

4.3.4 Remarks on the parameter study

The results of the parameter study are summarised in the diagram Figure 4-19. For the purpose of this section, the three stages of the M-ϕ and P-δ curves can be named as S1 for the pre-peak, S2 for the part immediately beyond peak and S3 for the third part of the curve.

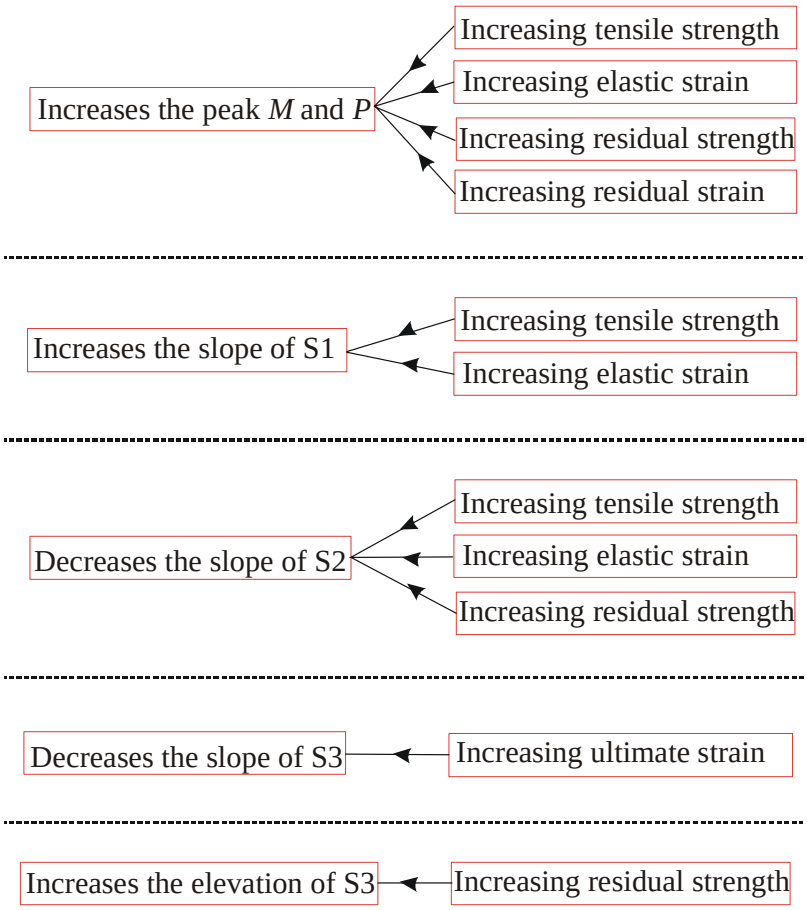

Figure 4-19: Summary of the parameter study.

The assumed σ-ε relationship was successfully used to calculate the M-ϕ and P-δ responses and therefore the process can be reversed to calculate a σ-ε relationship for SFRC if either the M-ϕ or P-δ response is available. In fact, the calculated σ-ε response will be more accurate if the M-ϕ response is used as fewer assumptions are involved in the analysis compared to the experimental P-δ response. However, measuring the P-δ response is relatively common and much simpler than measuring the M-ϕ response.

The parameter study highlighted that changing different parameters of the material can have a similar influence, but with different magnitude, on the M-ϕ and P-δ responses. For example, an increase in the peak load on the P-δ response can be achieved by changing one of four parameters as shown in Figure 4-19. However, the most significant influence on the M-ϕ and P-δ responses is obtained due to changes in the values of σ_{t0}. This is because the changes in the values of σ_{tu}, ε_{t0}, ε_{t1} and ε_{tu} are considered to be too small compared to possible changes in the value of σ_{t0}. It should not be deduced that the actual tensile σ-ε relationship for a particular SFRC is not unique as only one parameter of the σ-ε relationship is changed while keeping all the other parameters fixed.

However, these parameters are interrelated in some cases and therefore changing the value of one parameter leads to changes in the values of the other parameters. For example, changing the tensile and compressive strengths is expected to influence the residual strength. This is because the strength of concrete affects the characteristics of the fibre-matrix bond and thus influences the post-cracking behaviour of the SFRC. Although the σ-ε relationships used in this analysis might not represent realistic σ-ε responses, the results of the analysis are only indicative of the isolated effect of each of these parameters.

The method proposed here makes use of a small number of assumptions. The major assumption is the shape of the σ-ε relationship. The method can be applied to any selected σ-ε relationship that contains an appropriate number of parameters to model the observed typical M-ϕ or P-δ response. The proposed method is numerically demanding and therefore most suitable for computer applications. The numerical solution capabilities of programs such as Mathcad (2001) can greatly assist in the implementation of the method.

4.3.5 Initial estimation for the stress-strain relationship

An initial guess is required when determining the σ-ε relationship for SFRC. The initial guess will be adjusted using information obtained from the parameter study conducted here. Based on the experience gained from the analyses conducted in the previous sections, the following steps are recommended for calculation of the σ-ε relationship:

(1) Establish the compression σ-ε relationship. Make a first estimate for the tensile σ-ε response.

(2) Assuming Young's modulus is valid for tension too, adjust the peak M and peak P by changing σ_{t0}.

(3) Make adjustment to the elevation of S3 by changing σ_{tu}. This will slightly change peak M, peak P and the slope of S2.

(4) Make adjustments to the slope of S3 by changing ε_{tu}. This will slightly change the elevation.

(5) Make a small adjustment to the slope and elevation of S3 by adjusting the ε_{t1}. This will slightly change the peak M and peak P.

(6) Make final correction to the peak M, peak P and the slope of S1 by changing either ε_{t0} and / or σ_{t0}.

In step (1), the compression σ-ε relationship is established using the cube compressive strength (f_{cu}) and Young's modulus (E) for the FRC. The value of σ_{cu} and ε_{cu} can be approximated as f_{cu} and 0.0035 respectively. For the first estimate of the tensile σ-ε relationship, the following general guidelines can be used:

- For plain concrete, the ratio between uni-axial tensile and compressive strength usually ranges from 0.085 to 0.11 (Chen, 1982). Based on this ratio, the value of σ_{t0} for SFRC can be estimated as 0.1 times f_{cu} .
- Assume that Young's modulus generated from compression tests is valid for tension and calculate ε_{t0}.
- Estimate σ_{tu}, as a percentage of σ_{t0}. The estimation can be based on the ratio between flexural strength and the post-cracking strength values as provided by the steel fibre manufacturer. For example, σ_{tu} can be estimated as 42 percent of σ_{t0} if 15kg/m^3 of RC-80/60-BN hooked-end steel fibre is used, (Refer to the Table A-1 in Appendix A).
- Based on the recommendations of the RILEM TC 162-TDF (2002), the values of ε_{t1} and ε_{tu} can be estimated as $(\varepsilon_{t0} + 0.001)$ and 0.1 respectively.